

LETTER

Copiotrophic marine bacteria are associated with strong iron-binding ligand production during phytoplankton blooms

Shane L. Hogle,^{*1a} Randelle M. Bundy,^{1b} Jessica M. Blanton,² Eric E. Allen,² Katherine A. Barbeau¹

¹Geosciences Research Division, Scripps Institution of Oceanography, La Jolla, California; ²Marine Biology Research Division, Scripps Institution of Oceanography, La Jolla, California

Scientific Significance Statement

Organic ligands shape the marine biogeochemical cycle of iron by controlling its solubility in the ocean. The strongest of the detectable marine organic ligands are presumed to be produced by iron-limited marine microbes, but some field studies have shown that these same strong ligands paradoxically increase in concentration after iron fertilization when microbes are thought to be iron replete. Currently, the specific microbes and mechanisms responsible for increases in strong iron-binding ligands remain unknown. We present evidence that bacterial taxa typically associated with nutrient-rich environments are robustly associated with strong iron-binding ligands detected during the early stages of phytoplankton bloom collapse in experimental incubations. These results may potentially explain observations of spikes in strong ligand concentrations after iron additions in the field.

Abstract

Although marine bacteria were identified nearly two decades ago as potential sources for strong iron-binding organic ligands detected in seawater, specific linkages between ligands detected in natural water and the microbial community remain unclear. We compared the production of different classes of iron-binding ligands, dissolved iron and macronutrient concentrations, and phytoplankton and bacterioplankton assemblages in a series of iron amended 6-d incubations. Incubations with high iron additions had near complete macronutrient consumption and higher phytoplankton biomass compared with incubations with low iron additions, but both iron treatments were dominated by diatoms. However, we only detected the strongest ligands in high-iron treatments, and strong iron-binding ligands were generally correlated with an increased abundance of copiotrophic bacteria, particularly *Alteromonas* strains. Ultimately, these robust correlations suggest a potential linkage between copiotrophic bacteria and strong iron-binding ligand production after iron fertilization events in the marine environment.

*Correspondence: shogle@mit.edu

Present address:

^aDepartment of Civil and Environmental Engineering, Massachusetts Institute of Technology, Cambridge, Massachusetts, U.S.A

^bDepartment of Marine Chemistry and Geochemistry, Woods Hole Oceanographic Institution, Woods Hole, Massachusetts, U.S.A

Author Contribution Statement: SLH, RMB, EEA, and KAB designed research; SLH, RMB, JMB, and KAB performed research; SLH, JMB, and RMB analyzed data; SLH, RMB, and KAB wrote the article.

Data Availability Statement: Data and code for reproducing analyses are available from Figshare, Github, NCBI Bioproject Archive, NCBI Biosample Archive, and the NCBI Sequence Read Archive.

<https://dx.doi.org/10.6084/m9.figshare.3184534>

<https://github.com/slhogle/code-LO-letters-2016>

<http://www.ncbi.nlm.nih.gov/bioproject/PRJNA331054>

Additional Supporting Information may be found in the online version of this article.

This is an open access article under the terms of the Creative Commons Attribution License, which permits use, distribution and reproduction in any medium, provided the original work is properly cited.

The concentrations, chemical forms, and spatial/temporal distributions of oceanic iron are important factors shaping the ecology of marine phytoplankton and the overall productivity of marine ecosystems (Boyd et al. 2007). Dissolved iron (dFe) that has been regenerated from less kinetically labile forms, such as particles, is important in sustaining surface ocean productivity in iron-limited regions (Bowie et al. 2001). The mechanisms by which particulate iron is recycled back to dissolved iron and into the wider microbial food web, a process herein referred to as iron remineralization, are largely uncharacterized and represent major unknowns in global iron budgets (Tagliabue et al. 2016). The activity of microzooplankton (Barbeau et al. 2001) and viruses (Strzepek et al. 2005) are known to facilitate iron remineralization, and heterotrophic bacteria can also play a fundamental role (Boyd et al. 2010) as has been observed for other nutrients (Bidle and Azam 1999).

DFe is predominantly bound by organic ligands of mostly uncharacterized composition (Gledhill and van den Berg 1994; Rue and Bruland 1995). The concentrations and conditional stability constants, a measure of iron-binding strength, of natural marine ligands are typically measured using an electrochemical technique known as competitive ligand exchange—adsorptive cathodic stripping voltammetry (CLE-ACSV). Historically, organic ligands have been operationally partitioned into two classes based on their binding affinity for Fe (Gledhill and van den Berg 1994; Rue and Bruland 1995), but additional classes can be specified by varying the concentrations of a well-characterized competing ligand during electrochemical titrations, in a methodology termed Multiple Analytical Windows (MAW) (Bundy et al. 2014, 2015). Here, we partitioned organic ligands into three distinct classes in decreasing order of binding strength ($L_1 > L_2 > L_3$) using MAW and novel data processing techniques.

Some portion of the strong organic iron-binding ligands from seawater (Mawji et al. 2008) or marine cultures (Boiteau and Repeta 2015) are siderophores, bacterial secondary metabolites produced as an iron acquisition strategy. Intriguingly, the binding strengths of L_1 ligands measured in the field can be similar to or higher than those of known siderophores, leading to hypotheses that at least some portion of L_1 ligands in seawater may in fact be siderophores (Rue and Bruland 1995, 1997; Witter et al. 2000). Furthermore, electrochemical studies have demonstrated a positive correlation between L_1 ligand concentrations and biological activity as reviewed in Gledhill and Buck (2012), but the precise biological sources of those ligands are difficult to ascertain through electrochemical methods alone. Ultimately, it is clear that strong L_1 organic ligands are present in marine systems and are probably connected to the metabolic activities of marine bacteria and phytoplankton, but direct functional and mechanistic linkages between L_1 and biological community structure at this point remain elusive. Here, we couple high-throughput 16S rRNA marker gene surveys with MAW

CLE-ACSV chemical analysis in incubation experiments in order to explore how phytoplankton and bacterioplankton assemblage composition is connected to the production of different classes of iron-binding ligands.

Methods

Oceanographic setting and incubation setup

We collected trace-metal clean seawater for incubation experiments from 35 m depth in August 2012 approximately 250 km from the Southern California coast (33.879° N, 123.306° W). We sampled using 5 L Teflon-coated external-spring Niskin bottles on a rosette deployed on nonmetallic hydroline. After sampling, we moved Niskin bottles to a positive pressure clean van and dispensed unfiltered water into an acid-cleaned 50 L carboy. We added 10.0 $\mu\text{mol L}^{-1}$ NO_3^- , 1.0 $\mu\text{mol L}^{-1}$ PO_4^{3-} , and 9.3 $\mu\text{mol L}^{-1}$ Si(OH)_4 to the dispensed water and divided it between six 2.7 L polycarbonate bottles. Prior to use, we pretreated all macronutrients with Chelex resin to remove contaminating trace metals. We added 1 nmol L^{-1} FeCl_3 to Low Fe bottles and 5 nmol L^{-1} FeCl_3 to High Fe bottles then moved all bottles to an on-deck flow-through incubator screened to 30% incident light levels. We sampled bottles at 0 and 144 h (6 d) for dFe, dFe-binding ligands, chlorophyll *a* (chl *a*), macronutrients (NO_3^- , PO_4^{3-} , and Si(OH)_4), pigment concentrations, phytoplankton cell counts, and DNA and for only nutrients and chl *a* at 72, 120, and 144 h (days 3, 5, and 6). We sampled by rapidly moving incubation bottles to a trace metal clean van, subsampling bottles in a laminar flow hood, then returning bottles to the incubator.

Nutrients, pigments, and phytoplankton

We filtered subsamples (0.2 μm Acropak) of incubations, stored the flow through at -80°C , and measured Si(OH)_4 , PO_4^{3-} , and NO_3^- (nitrate + nitrite) onshore using a Lachat QuickChem 8000 flow injection analysis system. We collected samples for chl *a* and phytoplankton pigments onto GF/F filters, extracted the chl *a* filters in acetone for 24 h, and analyzed chl *a* concentrations fluorometrically on-board. We stored filters for accessory pigments in liquid N_2 until analysis by high performance liquid chromatography onshore. We preserved phytoplankton for cell counts in formalin and counted cells onshore using light microscopy. We classified cells by morphology into categories of *Chaetoceros* spp., *Pseudo-nitzschia* spp., other diatoms ($>10 \mu\text{m}$), dinoflagellates, flagellates ($<10 \mu\text{m}$), and ciliates.

Dissolved Fe and dFe-binding organic ligands

We analyzed total dFe using flow-injection analysis (FIA) as described by King and Barbeau (2007), and measured the concentration and conditional binding strengths of organic dFe-binding ligands using MAW CLE-CSV methods (Bundy et al. 2014, 2015, 2016). We resolved ligand classes using the ProMCC software and first attempted to fit our titration data

to three different ligand classes in a mass balance optimized speciation model (Omanović et al. 2015). If the model did not converge after 500 iterations, we fit the model again but for only two ligand classes. We characterized ligand classes as L_1 when $\log K_{\text{FeL1, Fe}'}^{\text{cond}} \geq 12.0$, L_2 when $\log K_{\text{FeL2, Fe}'}^{\text{cond}} = 11.0$ – 12.0 , and L_3 when $\log K_{\text{FeL3, Fe}'}^{\text{cond}} = 10.0$ – 11.0 . See Supporting Information for full sampling and methodological details.

DNA extraction, library preparation, and sequencing

We filtered 100 mL of seawater onto 0.22 μm Sterivex-GV filters (Millipore) without prefiltration and froze filters at -80°C . We extracted DNA onshore using the methods described by DeLong et al. (2006). We PCR amplified the V3-V4 region of the 16S ribosomal RNA gene from our samples using Q5 polymerase (New England Biolabs) and primers, S-D-Bact-0341-b-S-17/S-D-Bact-0785-a-A-21, (Klindworth et al. 2013) modified with Illumina adapters. We sequenced samples using 300 bp paired-end sequencing on an Illumina MiSeq machine running v3 chemistry, which generated an average of 1.2×10^5 reads per sample ($n = 6$) (Supporting Information Table S1).

OTU processing and analysis

Briefly an OTU or “Operational Taxonomic Unit” is a grouping of sequenced 16S ribosomal RNA read fragments with 97% nucleotide similarity. This classification cutoff has been traditionally assumed to correspond to microbial “species.” We merged paired reads from each sample using USEARCH v8.1.1861_i86linux32 (Edgar 2013), allowing no more than 1.0 total expected errors for all bases in the merged read (default parameters). We pooled, de-replicated, and grouped merged reads into OTUs at 97% sequence identity and removed chimeras by comparison to the UCHIME gold standard reference database. We then used the RDP Naïve Bayesian classifier (Wang et al. 2007) to taxonomically classify OTUs and remove unclassifiable OTUs at the kingdom level and OTUs matching eukaryotic, cyanobacterial, or archaeal sequences ($\sim 20\%$ of reads). We used the PhyloSeq package in R to process the resulting OTU abundance matrix (McMurdie and Holmes 2013) and tested for differential abundance of OTUs between treatments using DESeq2 (Love et al. 2014; McMurdie and Holmes 2014). See Supporting Information for data analysis procedures. All unix shell and R scripts for reproducing analyses can be downloaded from <https://dx.doi.org/10.6084/m9.figshare.3184534.v1>.

Results

Nutrients

The initial water for incubation experiments contained both low nitrate concentrations ($0.94 \mu\text{mol L}^{-1}$) and dFe concentrations ($0.31 \text{ nmol L}^{-1} \pm 0.04 \text{ nmol L}^{-1}$) (Supporting Information Tables S1, S2), indicating that the initial phytoplankton community was likely limited by NO_3^- (King and Barbeau 2007). For the nutrient amended incubations, we

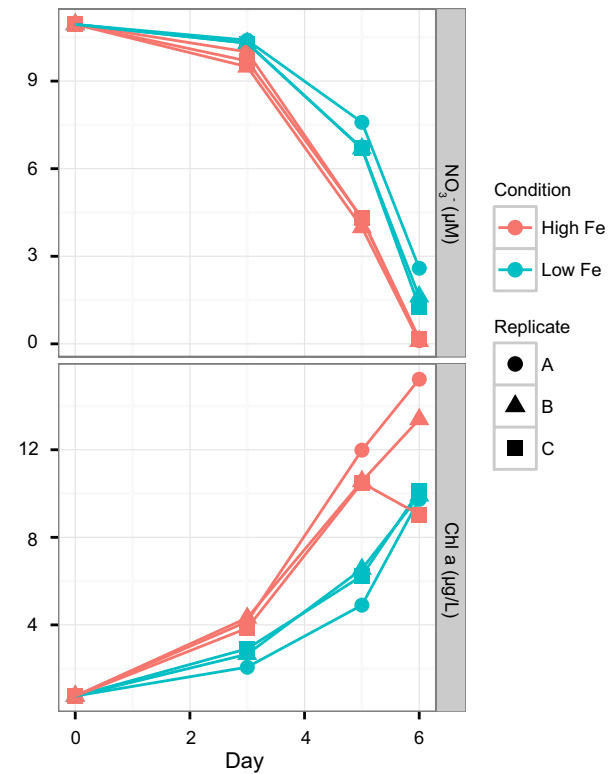


Fig. 1. Progression of Chlorophyll a (chl *a*) and nitrate (NO_3^-) concentrations during the course of the incubations. Nitrate concentrations at Day 0 are after the initial nutrient spike. High Fe incubations are in red, while Low Fe are in blue. Biological replicates are represented by different shapes. Note different scales in each subplot.

selected a low Low Fe treatment ($1 \text{ nmol L}^{-1} \text{ dFe}$, NO_3^- : $\text{dFe} = 9$) to simulate initial conditions approaching phytoplankton Fe-limitation and a High Fe treatment ($5 \text{ nmol L}^{-1} \text{ dFe}$, NO_3^- : $\text{dFe} = 2$) to simulate Fe-replete conditions. King and Barbeau (2007) determined that a nitrate to dFe ratio approaching 10 ($\mu\text{M NO}_3^-$: nM Fe) strongly indicated insufficient Fe to support complete phytoplankton nitrate consumption and consequently could be a reliable proxy for community Fe limitation in the field. After 6 d, average ratios of NO_3^- : dFe were elevated in Low Fe (NO_3^- : $\text{dFe} \cong 6$) relative to High Fe treatments (NO_3^- : $\text{dFe} \cong 0.2$) suggesting that Low Fe incubations were likely Fe stressed (Supporting Information Table S2).

Phytoplankton assemblage

The chl *a* concentration was initially $0.75 \mu\text{g L}^{-1}$, and increased to $9.91 \pm 0.18 \mu\text{g L}^{-1}$ in Low Fe treatments and $12.50 \pm 3.17 \mu\text{g L}^{-1}$ in High Fe treatments (Fig. 1). In both treatments, most of the biomass gain was due to an increase in the abundance of diatoms as indicated by the increase in fucoxanthin in Low Fe and High Fe incubations (Supporting Information Table S3) and direct observation in the cell counts (Supporting Information Table S4). Before Fe addition, the eukaryotic phytoplankton assemblage was composed

Table 1. Dissolved Fe-binding ligand concentrations.

Treatment	Day	DFe (nM)	DFe SD (nM)	L_1 (nM)	logK1	L_2 (nM)	logK2	L_3 (nM)	logK3
Initial	0	0.31	0.04	nd	nd	2.19	11.81	2.51	10.76
Low Fe A	6	0.31	0.02	nd	nd	2.55	11.82	3.79	10.20
Low Fe B	6	0.42	0.03	nd	nd	3.67	11.20	2.58	10.10
Low Fe C	6	0.21	0.02	nd	nd	4.10	11.74	3.65	10.20
High Fe A	6	0.61	0.04	4.39	12.02	2.97	11.38	6.58	10.10
High Fe B	6	0.62	0.17	3.65	12.36	3.07	11.00	7.54	9.39
High Fe C	6	0.60	0.06	2.54	12.08	3.57	11.16	4.60	10.16

Concentrations of DFe and DFe-binding ligands (L_x) in the six incubations after 6 d and at the start of the experiment (Day 0). Initial values are from in situ seawater used to start the incubations and do not include biological replicates. DFe is the total dissolved Fe concentration in nM, DFe SD is the standard deviation of three technical FIA replicates for the dissolved Fe measurements, $L_{(x)}$ is the concentration in nM of the three ligand classes defined in this study, LogK(x) displays \log_{10} of the conditional stability constant measured for each ligand class determined at the 95% confidence interval in chemical speciation mode in ProMCC with less than 10% root mean square error.

primarily of *Pseudo-nitzschia* species (67%) and other large diatoms. *Pseudo-nitzschia* spp. responded to Fe addition in both treatments, increasing to 78% of the assemblage on average in Low Fe bottles and 82% in High Fe bottles. Cell counts of specific taxonomic groups were not statistically different between High and Low Fe treatments when normalized to total cell counts, indicating that phytoplankton assemblage composition was largely unchanged between Fe treatments although total biomass increased in High Fe samples.

Dissolved Fe-binding ligands

We determined several classes of dFe-binding ligands in each experimental treatment, and Low Fe and High Fe treatments displayed different patterns after 6 d. L_2 and L_3 ligands were detected in situ in the initial water mass, while the strongest L_1 ligands were conspicuously absent (Table 1). After 6 d, Low and High Fe treatments displayed similar L_2 concentrations to initial CCE waters. L_3 concentrations increased at day 6 in High Fe compared with Low Fe treatments (Student's *t*-test, $p < 0.05$). However, the most striking result was the presence of strong L_1 ligands exclusively in High Fe treatments at day 6, while no Fe-binding ligands of this strength were detected in Low Fe treatments. In some treatments, the calculated logK of the L_1 class was similar to that of the L_2 class (within logK of 0.2). Although our rigorous data processing methodology resolved three High Fe ligand classes, it is possible that the L_1 and L_2 classes as defined in our study may have partially overlapped in High Fe samples. Regardless of overlapping binding strengths, there would still be significant ligand concentration difference between Low and High Fe treatments. These results suggest that L_1 production was dependent on Fe treatment and the resulting biological dynamics in these incubations.

Heterotrophic bacterial assemblage

We examined the composition of the heterotrophic bacterial assemblage in High and Low Fe treatments using 16S

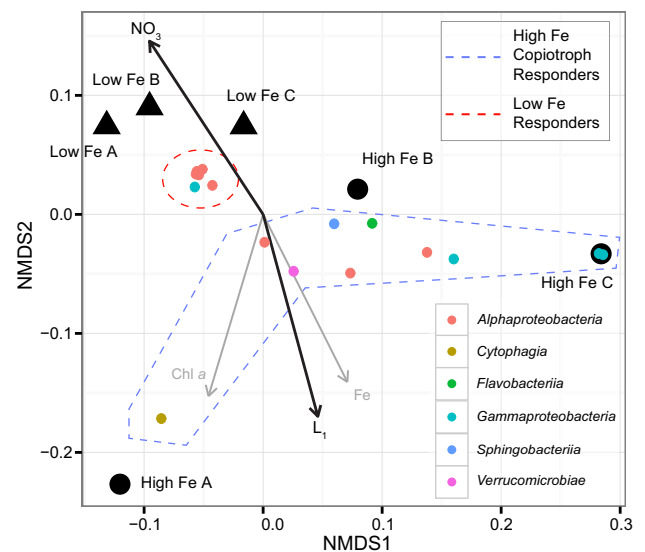


Fig. 2. Ordination plot of a NMDS analysis based on the diversity and abundance of bacterial OTUs detected at Day 6 of the experiment. The three High Fe samples (circles) and Low Fe samples (triangles) are plotted in addition to the ordination of individual OTUs (small colored circles). OTUs are colored according to the five most abundant taxonomic classes and only OTUs from Table 1 and Fig. 3 are displayed. Copiotroph OTUs responding to High Fe conditions are enclosed with a blue dashed line, while the red dashed line encompasses OTUs enriched in Low Fe samples. Arrows represent fitted vectors of continuous associated environmental variables and show the direction of the increasing gradient. Variables with a correlation p value < 0.1 are shown in black while those with $p > 0.1$ are shown in gray. Arrow length is proportional to the correlation between the variable and ordination. L_1 , $R^2 = 0.77$; Fe, $R^2 = 0.62$; chl *a*, $R^2 = 0.64$; NO_3^- , $R^2 = 0.75$.

rRNA marker gene sequencing. We first explored broad patterns of taxonomic diversity using a nonmetric multidimensional scaling (NMDS) analysis based on diversity and abundance of bacterial OTUs. This analysis indicated that Low Fe treatments were of a similar taxonomic composition, while High Fe treatments were largely variable between

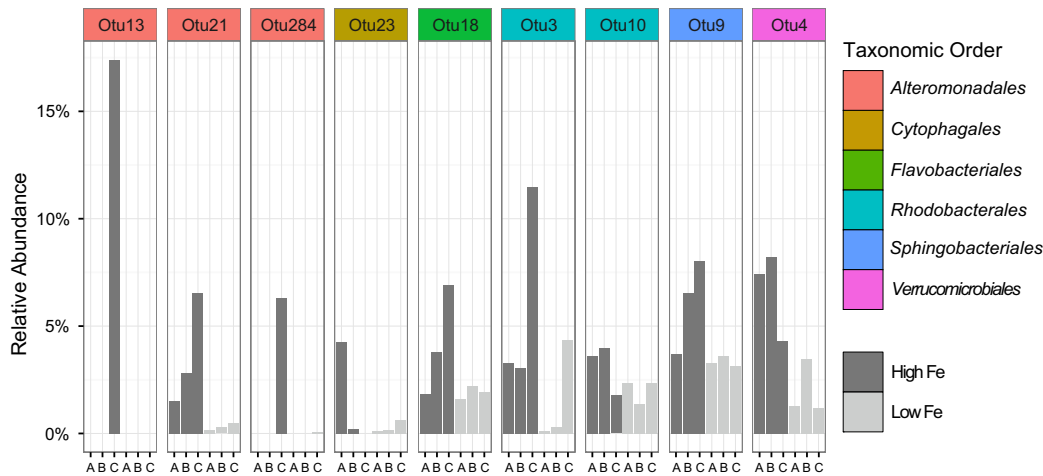


Fig. 3. Bar plot of copiotroph OTUs responding to High Fe conditions. Copiotroph OTUs have a mean relative abundance greater than 1% of all reads in each replicate and the High Fe mean is at least 1.5 times greater than the Low Fe mean. High Fe samples are dark gray while Low Fe samples are light gray.

Table 2. Differentially abundant OTUs between Fe treatments.

OTU	Base Mean	Log ₂ Fold Change	FDR adjusted <i>p</i> value	Class	Family	Genus
*Otu21	3340.45	-3.66	0.0006	<i>Gammaproteobacteria</i>	<i>Alteromonadaceae</i>	<i>Aestuariibacter</i>
*Otu78	133.98	-2.74	0.0001	<i>Alphaproteobacteria</i>	<i>Hyphomonadaceae</i>	<i>Hyphomonas</i>
*Otu4	5061.43	-2.17	0.0006	<i>Verrucomicrobiae</i>	<i>Rubritaleaceae</i>	<i>Rubritalea</i>
Otu2	7038.59	0.73	0.02	<i>Alphaproteobacteria</i>	<i>SAR11</i>	<i>Pelagibacter</i>
Otu245	109.48	1.06	0.03	<i>Alphaproteobacteria</i>	<i>SAR11</i>	<i>Pelagibacter</i>
Otu45	248.55	1.08	0.04	<i>Alphaproteobacteria</i>	<i>Rhodobacteraceae</i>	<i>Roseibacterium</i>
Otu32	1146.14	1.18	0.01	<i>Alphaproteobacteria</i>	<i>SAR11</i>	<i>Pelagibacter</i>
Otu57	119.82	1.21	0.002	<i>Alphaproteobacteria</i>	<i>Kordiimonadaceae</i>	<i>Kordiimonas</i>
Otu56	212.94	1.23	0.02	<i>Gammaproteobacteria</i>	<i>Oleiphilaceae</i>	<i>Oleiphilus</i>
Otu15	1776.33	1.52	0.01	<i>Flavobacteriia</i>	<i>Flavobacteriaceae</i>	<i>Corallibacter</i>

Significant differential abundances of OTUs between high and low Fe conditions after 6 d. Asterisks denote taxa considered to be copiotrophic responders to High Fe treatments. Only OTUs with false discovery rate corrected *p* values less than 0.05 and with base means greater than 100 are displayed. Base mean indicates the mean OTU abundance across all samples. Log₂ Fold Change is the fold change from high Fe to low Fe samples (i.e., a negative value indicates enrichment in high Fe samples) and OTUs are ordered by increasing fold change, FDR adjusted *p* value is the False Discovery Rate adjusted *p* value from negative binomial Wald Tests for significant differential abundance between Fe treatments, and the remaining columns designate taxonomic class, family, and genus of each OTU.

replicates but also taxonomically distinct from Low Fe incubations (Fig. 2). We then fit continuous environmental variables to the OTU ordination and tested for correlations at a significance level of $\alpha = 0.1$. Increasing NO₃⁻ concentrations were positively correlated with the bacterial OTU composition in Low Fe incubations ($R^2 = 0.75$, $p < 0.05$), while L_1 concentrations were strongly positively correlated with OTUs more abundant in High Fe treatments (L_1 , $R^2 = 0.77$, $p < 0.05$). The alpha diversity, or the total species richness in each incubation, was significantly lower in High Fe treatments (Supporting Information Table S5).

Because we were struck by the differences in L_1 concentrations between Fe treatments and the general alignment of

the OTU composition with increasing L_1 , we searched for potential indicator OTUs that were abundant and overrepresented in High Fe incubations. We narrowed our search to OTUs that each comprised greater than 1% of the total reads in each sample and also had average abundances that were at minimum 1.5 times greater in High Fe samples than in Low Fe samples. Nine OTUs matched these criteria, and all were similar to known copiotrophic strains particularly from the orders *Alteromonadales* and *Rhodobacterales* (Fig. 3, Supporting Information Table S6). We also tested for differentially abundant OTUs using a mixture model framework (Love et al. 2014) which identified ten OTUs (Table 2) with a statistically significant difference in abundance between

High and Low Fe treatments. Three of these OTUs were enriched in High Fe incubations and had strong similarity to copiotrophic strains. Some highly abundant copiotrophic OTUs, for example *Alteromonas* OTU13, co-occurred almost exclusively with a single replicate from High Fe treatments (Fig. 3) and were missed by the mixed model approach due to their large variability.

Discussion

After 6 d of incubation, both High and Low Fe treatments stimulated phytoplankton biomass and produced diatom blooms. However, the phytoplankton assemblages in High and Low Fe treatments were largely of the same taxonomic composition, while the Fe-binding ligand pool, macronutrient concentrations, and the heterotrophic microbial assemblage differed substantially. The strongest L_1 ligands were particularly distinct between Fe treatments, and the L_1 ligand classification, defined in this study as having a $\log K \geq 12$, is comparable with the binding affinities of siderophores found in cultures of marine bacteria (Vraspir and Butler 2009). Siderophores are a probable constituent of the operationally defined L_1 class defined here, but we stress that the L_1 class should not be considered to be entirely composed of siderophores.

One possible explanation for the emergence of strong L_1 ligands in High Fe treatments is that they were produced actively by phytoplankton. However, sequenced eukaryotic phytoplankton genomes lack siderophore biosynthesis pathways and do not appear directly take up siderophores (Morrissey and Bowler 2012). An alternative explanation for differences in L_1 is from variation in the composition and activities of bacteria. The bacterial assemblage in High Fe incubations was broadly aligned with L_1 concentrations, and these incubations were dominated by a handful of OTUs related to copiotrophic strains (Supporting Information Table S6). This copiotroph enrichment was also reflected by the reduced species richness in High Fe treatments (Supporting Information Table S5). Although we only detected L_1 in High Fe incubations, replicates had variable L_1 concentrations as well as variable abundances of copiotroph OTUs (Figs. 2, 3), which may reflect unsampled ecological dimensions from our study. This could include differences in the concentrations and types of bacterial growth substrates in each replicate (Goutx et al. 2007; Mayali et al. 2015), potentially antagonistic microbial interactions (Long and Azam 2001), and/or that multiple copiotrophic groups may produce strong organic ligands. Despite the intravariability of High Fe replicates, broad patterns in the composition of the heterotrophic microbial assemblage appeared to align with the High/Low Fe treatment experimental structure (Fig. 2).

Our observations are consistent with other studies reporting an enrichment of generalist, copiotrophic bacterial taxa after dissolved organic matter additions, and biogenic particle additions to seawater (Nelson and Carlson 2012; Mayali et al.

2015). Other studies have demonstrated that the activities of mostly rare but transiently abundant and transcriptionally active marine copiotrophic bacteria have disproportionately large impacts on biogeochemical cycling (Pedler et al. 2014). Copiotrophic microbial taxa tend to have large genomes with greater regulatory capacity and a greater diversity of Fe acquisition pathways including siderophore biosynthesis and/or siderophore uptake (Hogle et al. 2016). Copiotrophs can also rapidly adapt to patchy nutrient conditions and exploit diverse growth substrates. It may be that copiotrophs also have a large Fe demand in order to fuel their rapid growth and carbon consumption after episodic nutrient pulses. For example, hydroxamate siderophore production by *Pseudoalteromonas haloplanktis* is sensitive to carbon availability (Sijerčić and Price 2015), and the *Alteromonas* sp. ALT199 genome contains a petrobactin biosynthesis pathway (Pedler et al. 2014).

We suggest that the most likely scenario accounting for the emergence of L_1 in High Fe treatments is that copiotrophic bacteria were directly producing strong Fe-binding organic ligands in order to scavenge iron from lysing algal cells. The almost complete drawdown of nitrate in all High Fe replicates and the chl *a* collapse in High Fe C suggests that after 6 d the phytoplankton assemblage in High Fe treatments had entered or was beginning to enter the initial phases of remineralization. We postulate that phytoplankton senescence was coupled with a release of dissolved organic matter (DOM) which stimulated endemic bacterial copiotrophs (Buchan et al. 2014). We suspect the differences between Low and High Fe treatments in the bacterial assemblages were primarily driven by DOM, while the differences in L_1 concentrations reflected siderophore and other strong organic ligand production by copiotrophs responding to DOM enrichment. Although this study provides only correlative evidence and limited temporal resolution, our results do suggest a potential link between specific copiotrophic bacteria and strong dFe-binding ligand production and further study is warranted.

Large scale Fe fertilization studies have demonstrated increases in strong dFe-binding ligands when microbial communities were presumably Fe replete (Rue and Bruland 1997) as well as during phytoplankton bloom decline after Fe fertilization (Kondo et al. 2008). Our experiments suggest that spikes of L_1 production in these mesoscale studies may have been related to shifts in copiotrophic bacterial abundance during phytoplankton blooms. We hypothesize that high Fe conditions initially stimulate Fe-limited photoautotrophs, particularly diatoms, but not endemic heterotrophic bacteria due to organic carbon limitation (Kirchman 1990; Church et al. 2000). As the diatom bloom exhausts inorganic nutrients and progresses to senescence, newly released diatom-derived DOM associated with algal senescence stimulates ambient carbon-limited copiotroph bacteria (Seyedsayamdost et al. 2011; Sule and Belas 2013). Because aerobic respiration requires many Fe-containing enzymes (Hogle et al. 2014), rapidly growing

copiotrophs may quickly shift to Fe limitation relative to excess algal-derived organic carbon. The most abundant local Fe source in this context would likely be algal-derived metalloproteins, and copiotroph L_1 production may function to extract Fe from these algal sources and make it bioavailable to the wider bacterial community. If this phenomenon is widespread it may serve as a significant source of strong organic ligands in marine waters. Strong ligand production by heterotrophic bacteria during early bloom senescence may thus be important for overall iron recycling efficiency in microbial ecosystems and may serve to reduce Fe loss due to particle export in the upper ocean.

References

- Barbeau, K., E. Kujawinski, and J. Moffett. 2001. Remineralization and recycling of iron, thorium and organic carbon by heterotrophic marine protists in culture. *Aquat. Microb. Ecol.* **24**: 69–81.
- Bidle, K. D., and F. Azam. 1999. Accelerated dissolution of diatom silica by marine bacterial assemblages. *Nature* **397**: 508–512.
- Boiteau, R. M., and D. J. Repeta. 2015. An extended siderophore suite from *Synechococcus* sp. PCC 7002 revealed by LC-ICPMS-ESIMS. *Metallomics* **7**: 877–884. doi:10.1039/C5MT00005J
- Bowie, A. R., M. T. Maldonado, R. D. Frew, and others. 2001. The fate of added iron during a mesoscale fertilisation experiment in the Southern Ocean. *Deep Sea Res. Part 2 Top. Stud. Oceanogr.* **48**: 2703–2743.
- Boyd, P. W., T. Jickells, C. S. Law, and others. 2007. Mesoscale iron enrichment experiments 1993–2005: Synthesis and future directions. *Science* **315**: 612–617.
- Boyd, P. W., E. Ibsanmi, S. G. Sander, K. A. Hunter, and G. A. Jackson. 2010. Remineralization of upper ocean particles: Implications for iron biogeochemistry. *Limnol. Oceanogr.* **55**: 1271–1288.
- Buchan, A., G. R. LeClerc, C. A. Gulvik, and J. M. González. 2014. Master recyclers: Features and functions of bacteria associated with phytoplankton blooms. *Nat. Rev. Microbiol.* **12**: 686–698.
- Bundy, R. M., D. V. Biller, K. N. Buck, K. W. Bruland, and K. A. Barbeau. 2014. Distinct pools of dissolved iron-binding ligands in the surface and benthic boundary layer of the California current. *Limnol. Oceanogr.* **59**: 769–787.
- Bundy, R. M., H. A. N. Abdulla, P. G. Hatcher, D. V. Biller, K. N. Buck, and K. A. Barbeau. 2015. Iron-binding ligands and humic substances in the San Francisco Bay estuary and estuarine-influenced shelf regions of coastal California. *Mar. Chem.* **173**: 183–194.
- Bundy, R. M., M. Jiang, M. Carter, and K. A. Barbeau. 2016. Iron-binding ligands in the Southern California Current System: Mechanistic studies. *Front. Mar. Sci.* **3**: article 27, 1–17. doi:10.3389/fmars.2016.00027
- Church, M. J., D. A. Hutchins, and H. W. Ducklow. 2000. Limitation of bacterial growth by dissolved organic matter and iron in the Southern ocean. *Appl. Environ. Microbiol.* **66**: 455–466. doi:10.1128/AEM.66.2.455-466.2000
- DeLong, E. F., C. M. Preston, T. Mincer, and others. 2006. Community genomics among stratified microbial assemblages in the ocean's interior. *Science* **311**: 496–503.
- Edgar, R. C. 2013. UPARSE: Highly accurate OTU sequences from microbial amplicon reads. *Nat. Methods* **10**: 996–998.
- Gledhill, M., and C. M. G. van den Berg. 1994. Determination of complexation of iron(III) with natural organic complexing ligands in seawater using cathodic stripping voltammetry. *Mar. Chem.* **47**: 41–54.
- Gledhill, M., and K. N. Buck. 2012. The organic complexation of iron in the marine environment: A review. *Front. Microbiol.* **3**: 69.
- Goutx, M., S. G. Wakeham, C. Lee, and others. 2007. Composition and degradation of marine particles with different settling velocities in the northwestern Mediterranean Sea. *Limnol. Oceanogr.* **52**: 1645–1664.
- Hogle, S. L., K. A. Barbeau, and M. Gledhill. 2014. Heme in the marine environment: From cells to the iron cycle. *Metallomics* **6**: 1107–1120.
- Hogle, S. L., J. Cameron Thrash, C. L. Dupont, and K. A. Barbeau. 2016. Trace metal acquisition by marine heterotrophic bacterioplankton with contrasting trophic strategies. *Appl. Environ. Microbiol.* **82**: 1613–1624.
- King, A. L., and K. Barbeau. 2007. Evidence for phytoplankton iron limitation in the southern California Current System. *Mar. Ecol. Prog. Ser.* **342**: 91–103.
- Kirchman, D. L. 1990. Limitation of bacterial growth by dissolved organic matter in the subarctic Pacific. *Mar. Ecol. Prog. Ser.* **62**: 47–54.
- Klindworth, A., E. Pruesse, T. Schweer, J. Peplies, C. Quast, M. Horn, and F. O. Glöckner. 2013. Evaluation of general 16S ribosomal RNA gene PCR primers for classical and next-generation sequencing-based diversity studies. *Nucleic Acids Res.* **41**: e1.
- Kondo, Y., S. Takeda, J. Nishioka, H. Obata, K. Furuya, W. K. Johnson, and C. S. Wong. 2008. Organic iron (III) complexing ligands during an iron enrichment experiment in the western subarctic North Pacific. *Geophys. Res. Lett.* **35**: L12601.
- Long, R. A., and F. Azam. 2001. Antagonistic interactions among marine pelagic bacteria. *Appl. Environ. Microbiol.* **67**: 4975–4983.
- Love, M. I., W. Huber, and S. Anders. 2014. Fully formatted moderated estimation of fold change and dispersion for RNA-seq data with DESeq2. *Genome Biol.* **15**: 1–21.
- Mawji, E., M. Gledhill, J. A. Milton, and others. 2008. Hydroxamate siderophores: Occurrence and importance in the Atlantic Ocean. *Environ. Sci. Technol.* **42**: 8675–8680. doi:10.1021/es801884r

- Mayali, X., B. Stewart, S. Mabery, and P. K. Weber. 2015. Temporal succession in carbon incorporation from macromolecules by particle-attached bacteria in marine microcosms. *Environ. Microbiol. Rep.* **8**: 68–75. doi:[10.1111/1758-2229.12352](https://doi.org/10.1111/1758-2229.12352)
- McMurdie, P. J., and S. Holmes. 2013. Phyloseq: An R package for reproducible interactive analysis and graphics of microbiome census data. *PLoS One* **8**: e61217. doi:[10.1371/journal.pone.0061217](https://doi.org/10.1371/journal.pone.0061217)
- McMurdie, P. J., and S. Holmes. 2014. Waste not, want not: Why rarefying microbiome data is inadmissible. *PLoS Comput. Biol.* **10**: e1003531. doi:[10.1371/journal.pcbi.1003531](https://doi.org/10.1371/journal.pcbi.1003531)
- Morrissey, J., and C. Bowler. 2012. Iron utilization in marine cyanobacteria and eukaryotic algae. *Front. Microbiol.* **3**: 43.
- Nelson, C. E., and C. A. Carlson. 2012. Tracking differential incorporation of dissolved organic carbon types among diverse lineages of Sargasso Sea bacterioplankton. *Environ. Microbiol.* **14**: 1500–1516.
- Omanović, D., C. Garnier, and I. Pižeta. 2015. ProMCC: An all-in-one tool for trace metal complexation studies. *Mar. Chem.* **173**: 25–39.
- Pedler, B. E., L. I. Aluwihare, and F. Azam. 2014. Single bacterial strain capable of significant contribution to carbon cycling in the surface ocean. *Proc. Natl. Acad. Sci. USA* **111**: 7202–7207.
- Rue, E. L., and K. W. Bruland. 1995. Complexation of iron(-III) by natural organic ligands in the Central North Pacific as determined by a new competitive ligand equilibration/adsorptive cathodic stripping voltammetric method. *Mar. Chem.* **50**: 117–138.
- Rue, E. L., and K. W. Bruland. 1997. The role of organic complexation on ambient iron chemistry in the equatorial Pacific Ocean and the response of a mesoscale iron addition experiment. *Limnol. Oceanogr.* **42**: 901–910.
- Seyedsayamdost, M. R., G. Carr, R. Kolter, and J. Clardy. 2011. Roseobacticides: Small molecule modulators of an algal-bacterial symbiosis. *J. Am. Chem. Soc.* **133**: 18343–18349.
- Sijerčić, A., and N. M. Price. 2015. Hydroxamate siderophore secretion by *Pseudoalteromonas haloplanktis* during steady-state and transient growth under iron limitation. *Mar. Ecol. Prog. Ser.* **531**: 105–120.
- Strzepek, R. F., M. T. Maldonado, J. L. Higgins, J. Hall, K. Safi, S. W. Wilhelm, and P. W. Boyd. 2005. Spinning the “Ferrous Wheel”: The importance of the microbial community in an iron budget during the FeCycle experiment. *Glob. Biogeochem. Cycles* **19**:1–14.
- Sule, P., and R. Belas. 2013. A novel inducer of roseobacter motility is also a disruptor of algal symbiosis. *J. Bacteriol.* **195**: 637–646.
- Tagliabue, A., O. Aumont, R. DeAth, and others. 2016. How well do global ocean biogeochemistry models simulate dissolved iron distributions? *Glob. Biogeochem. Cycles* **30**: 149–174. doi:[10.1002/2015GB005289](https://doi.org/10.1002/2015GB005289)
- Vraspir, J. M., and A. Butler. 2009. Chemistry of marine ligands and siderophores. *Ann. Rev. Mar. Sci.* **1**: 43–63.
- Wang, Q., G. M. Garrity, J. M. Tiedje, and J. R. Cole. 2007. Naïve Bayesian classifier for rapid assignment of rRNA sequences into the new bacterial taxonomy. *Appl. Environ. Microbiol.* **73**: 5261–5267.
- Witter, A. E., D. A. Hutchins, A. Butler, and G. W. Luther. 2000. Determination of conditional stability constants and kinetic constants for strong model Fe-binding ligands in seawater. *Mar. Chem.* **69**: 1–17.

Acknowledgments

We thank Christopher Rivera for help with Illumina library preparation, Jeff Hasty at UCSD for use of his MiSeq system, and Melissa Carter at SIO for phytoplankton cell counts. This work was funded by NSF GRFP grant DGE-144086 to SLH and NSF grants OCE-1061068 and OCE-1558841 to KAB. We thank the participants of the California Current Ecosystem Long Term Ecological Research program (NSF OCE-1026607) and the captain and the crew of the R/V Melville. The funders had no role in study design, data collection and interpretation, or the decision to submit the work for publication.

Submitted 12 May 2016

Revised 16 August 2016

Accepted 22 August 2016